### 4.4.8 Change of nondimensionalization

We thought after the discussion of the basic balance of convection in section 4.2, that it was logical to use a Stokes velocity $V_0$, to normalize the equations. We have therefore introduced a velocity and a time of order of 300 m yr$^{-1}$ and of $a/V_0$=10000 yr (see Table 1). This is certainly very fast or short compared with geological scales. Most physical and geophysical textbooks (e.g., *Schubert et al.*, 2001) use instead a diffusive time $t_D = \rho C_P a^2/k_0$ and velocity $a/t_D$. This is perfectly valid but Table 1, shows that the diffusive time and velocity amount to $t_D = 400$ byr and $V_D = 7\ 10^{-6}$ m yr$^{-1}$. This is even less Earth-like which means that the nondimensionalized values using a diffusive time may have rather unequal orders of magnitude. Using this approach, we would have obtained the anelastic equations

$$
\begin{aligned}
\tilde{\boldsymbol{\nabla}} \cdot (\frac{\bar{\rho}}{\rho_0}\tilde{\mathbf{v}}) =& 0. \\
\frac{1}{Pr}\frac{D\tilde{\mathbf{v}}}{D\tilde{t}} =& -\tilde{\boldsymbol{\nabla}}\tilde{P} + \tilde{\boldsymbol{\nabla}}\cdot\tilde{\tau} + \frac{\bar{\rho}}{\rho_0}\frac{\bar{\mathbf{g}}}{g_0}\frac{K_T^0}{\bar{K}_T}\frac{D_0}{\Gamma_0}\frac{C_P^0}{C_V^0}\tilde{P} - \frac{\bar{\rho}}{\rho_0}\frac{\bar{\mathbf{g}}}{g_0}\frac{\bar{\alpha}}{\alpha_0}Ra\tilde{T} \\
\frac{\bar{\rho}}{\rho_0}\frac{\bar{C}_P}{C_P^0}\frac{D\tilde{T}}{D\tilde{t}} =& \tilde{\boldsymbol{\nabla}}\cdot\left[\frac{\bar{k}}{k_0}\tilde{\boldsymbol{\nabla}}\left(\frac{\bar{T}}{\Delta T}+\tilde{T}\right)\right] + \\
& \frac{\bar{\alpha}}{\alpha_0}\frac{\bar{\rho}}{\rho_0}\frac{\bar{g}}{g_0}D_0\tilde{T}\tilde{v}_g + \frac{\bar{\rho}}{\rho_0}\frac{\rho_0 H a^2}{k_0\Delta T} + \frac{D_0}{Ra}\tilde{\underline{\boldsymbol{\tau}}} : \tilde{\boldsymbol{\nabla}}\tilde{\mathbf{v}}
\end{aligned}
\tag{135}
$$

and the Boussinesq equations,

$$
\begin{aligned}
\tilde{\boldsymbol{\nabla}}\cdot\tilde{v} =& 0, \\
\frac{1}{Pr}\frac{D\tilde{\mathbf{v}}}{D\tilde{t}} =& -\tilde{\boldsymbol{\nabla}}\tilde{P} + \tilde{\boldsymbol{\nabla}}\cdot\left(\frac{\mu}{\mu_0}(\tilde{\boldsymbol{\nabla}}\tilde{\mathbf{v}} + [\tilde{\boldsymbol{\nabla}}\tilde{\mathbf{v}}]^t)\right) - \frac{\bar{\mathbf{g}}}{g_0}\frac{\bar{\alpha}}{\alpha_0}Ra\tilde{T}, \\
\frac{D\tilde{T}}{D\tilde{t}} =& \tilde{\boldsymbol{\nabla}}\cdot\left[\frac{\bar{k}}{k_0}\tilde{\boldsymbol{\nabla}}\tilde{T}\right] + \frac{1}{Ra}\frac{\rho_0 H a^2}{k_0\Delta T}.
\end{aligned}
\tag{136}
$$

Notice that the $Ra$ number appears in different places than in (125) or (131). Of course after their appropriate changes of variables the solutions back with real dimensions are the same.

## 4.5 Linear stability analysis for basally heated convection

Using the Boussinesq approximation, it is easy to understand why the diffusive solution is not necessarily the solution chosen by the fluid. The standard way to test the stability of a solution is what physicists call a study of marginal stability (see also Chapter 5). It consists of substituing into the basic equations a known

solution plus an infinitely small perturbation and checking whether or not this perturbation amplifies, decreases or propagates. Its is only if the perturbation decreases in amplitude, that the tested solution is stable.

Since we benefit from the assumption that the perturbation has initially an infinitely small amplitude, computing its time evolution is simpler than solving the general equations since the nonlinear products can be neglected. The marginal stability study is therefore powerful for mapping the stability domain of a solution and describing its destabilization. At the same time it is also somewhat frustrating as the real unstable solution cannot be obtained.

This approach can be employed to understand the destabilisation of the diffusive solution. We use the Boussinesq approximation, with constant viscosity and conductivity, neglecting inertia and without internal heating. The nondimensionalized equations (131) (the tilde sign has been omitted for simplicity) write

$$\begin{aligned} \boldsymbol{\nabla}\cdot\mathbf{v} &= 0, \\ -\boldsymbol{\nabla}P + \boldsymbol{\nabla}^2\mathbf{v} - T\mathbf{e}_z &= 0, \\ \frac{\partial T}{\partial t} + \mathbf{v}\cdot\boldsymbol{\nabla}T &= \frac{1}{Ra}\boldsymbol{\nabla}^2 T, \end{aligned} \tag{137}$$

($\mathbf{e}_z$ is a normal vector directed along $\mathbf{g}$). The steady diffusive nondimensional temperature solution is $T = z$ with $z$ directed along $\mathbf{g}$, and we test a solution of the form $T = z+\delta T$. The temperature boundary condition, $T = 0$ on top and $T = 1$ at the bottom requires that $\delta T$ vanishes for $z = 0$ and $z = 1$. As in the diffusive case the velocity is zero, the velocity induced by $\delta T$ will be infinitely small $\delta\mathbf{v}$. In the nonlinear term, we can do the approximation $\mathbf{v}\cdot\boldsymbol{\nabla}T = \delta\mathbf{v}\cdot\boldsymbol{\nabla}(z+\delta T) \sim \delta v_z = v_z$. With this approximation, the equations are linear and we can find a solution in the form of a plane wave.

For a fluid confined between $z = 0$ and $z = 1$ and unbounded in the $x$-direction, a solution, $\delta T = \theta(t)\sin(\pi z)\sin(kx)$ is appropriate and satisfies the boundary conditions. This solution is 2D, has a single mode in the $z$-direction, and is periodic in $x$ with wavelength $\lambda = 2\pi/k$. More complex patterns could be tried but the mode we have chosen would destabilize first (see Chapter 5). It is then straightforward to deduce that for such a thermal anomaly, the energy equation imposes a vertical velocity

$$v_z = -\left(\dot{\theta} + \frac{(k^2+\pi^2)}{Ra}\theta\right)\sin(\pi z)\sin(kx). \tag{138}$$

From mass conservation the $x$-component of the velocity must be

$$v_x = -\frac{\pi}{k}\left(\dot{\theta} + \frac{(k^2+\pi^2)}{Ra}\theta\right)\cos(\pi z)\cos(kx). \tag{139}$$

This flow has a vertical component that vanishes on the top and bottom surfaces where the horizontal component is maximum. The choice of the temperature structure corresponds to free-slip velocity conditions. When the velocity and the temperature are introduced in the momentum equation, the time evolution of the temperature perturbation is found

$$\dot{\theta} = \theta \left( \frac{k^2}{(\pi^2 + k^2)^2} - \frac{(\pi^2 + k^2)}{Ra} \right). \tag{140}$$

For any wavenumber $k$, a small enough Rayleigh number corresponds to a stable solution, $\dot{\theta}/\theta < 0$. When the Rayleigh number is increased, the temperature component of wavenumber $k$ becomes unstable at the threshold Rayleigh

$$Ra = \frac{(\pi^2 + k^2)^3}{k^2}. \tag{141}$$

This $Ra(k)$ curve is plotted in Fig 3. This curve has a minimum when

$$k = \frac{\pi}{\sqrt{2}}, \quad Ra_c = \frac{27}{4}\pi^4 \sim 657. \tag{142}$$

What can be interpreted as the size of one convective cell is $\pi/k$ since one wavelength corresponds to two contrarotating cells. The critical cell has an aspect ratio, width over height, of $\sqrt{2}$.

A Rayleigh number of 657 is the critical Rayleigh number for convection heated from below with free-slip boundary conditions. As soon as $Ra > Ra_c$ there is a wavenumber interval over which convection begins. Of course, when convection grows in amplitude, the marginal stability solution becomes less and less pertinent as the assumption that $\delta v \cdot \boldsymbol{\nabla} \delta T << \delta v \cdot \boldsymbol{\nabla} z$ becomes invalid.

## 4.6 Road to chaos

Following the same approach, but with some additional complexities, the critical Rayleigh number for convection between no-slip surfaces, mixed free-slip/no-slip, with internal heating in Cartesian and spherical geometries could be obtained (e.g., see *Schubert et al.* (2001)). In all cases, critical Rayleigh numbers of order of $10^3$ are found.

In Cartesian geometry, when the Rayleigh number reaches its critical value, convection starts, and forms rolls. When the Rayleigh number is further increased, complex series of convection patterns can be obtained, first stationary, then periodic, anf finally, chaotic. Using the values of Table 1, the critical Rayleigh number of the mantle would be attained for a non-adiabatic temperature difference between the surface and the CMB of only 0.025 K! The mantle Rayleigh number

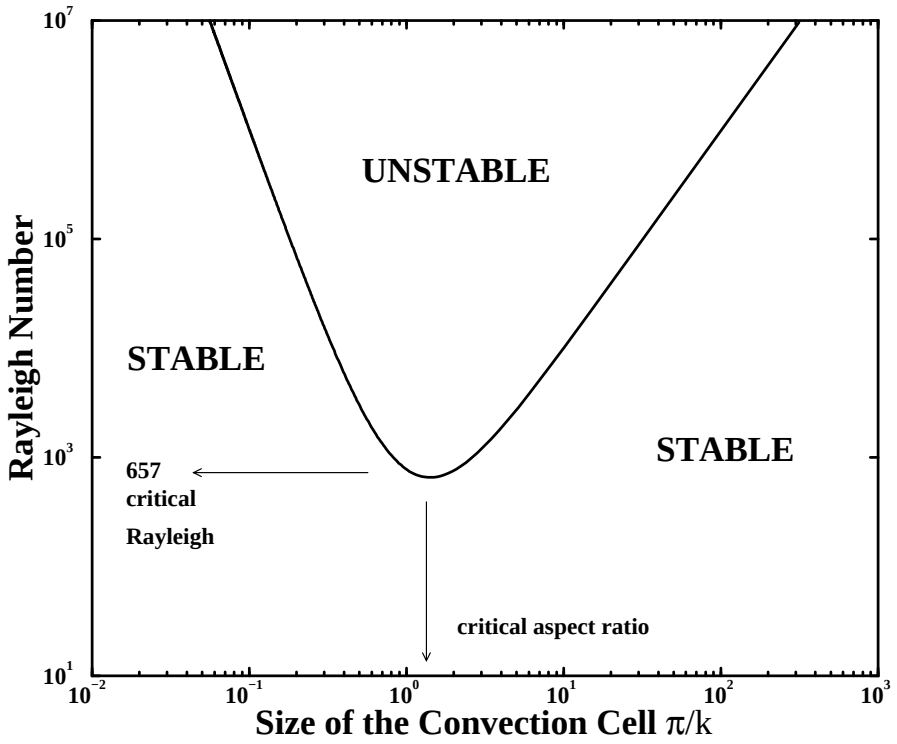


Figure 3: Critical Rayleigh number as a function of the half wavelength $\pi/k$ (the size of the convection cells). Above this curve, convection occurs with a whole range of unstable wavelengths. Below this curve, the conductive temperature is stable since temperature perturbations of any wavelength, decrease. When the Rayleigh number is increased, the first unstable wavelength corresponds to a convection cell of aspect ratio $\sqrt{2}$ and a critical Rayleigh number of 657.

is orders of magnitude higher than critical and the mantle is in a chaotic state of convection.

Figure 4 shows a stationary convection pattern at $Ra = 10^5$ and three snapshots of numerical simulation of convection at higher Rayleigh number. The color scale has been chosen differently in each panel to emphasize the thermal structures that decrease in length scale with $Ra$. This view is somewhat misleading since all the thermal anomalies become confined in a top cold boundary layer and in a hot bottom one at large Rayleigh numbers. Most of the interior of the cell becomes just isothermal (or adiabatic when anelastic equations are used). The various transitions of convection as the Rayleigh number increases will be discussed in other chapters of this Treatise (see e.g., Chapter 4).

# 5 Introduction to physics of multicomponent and multiphase flows

The mantle is not a simple homogeneous material. It is made of grains of variable bulk composition and mineralogy and contains fluids, magma and gases. Discussion of multicomponent and multiphase flows could deal with solids, liquids or gases, include compressibility or not, and consider elastic, viscous or more complex rheology. For each combination of these characteristics a geophysical application is possible. Here we will restrict the presentation to viscous creep models (i.e., without inertia), where the various components are treated with continuous variables (i.e., each component is implicitly present everywhere). We do not consider approaches where the various components are separated by moving and deformable interfaces. Our presentation excludes cases where the problem is to match properties at macroscopic interfaces between regions of different but homogeneous compositions.

We will focus on two cases. First, when all the components are perfectly mixed in variable proportions. This corresponds to the classical chemical approach of multiple components in a solution. This will provide some tools to understand mantle phase transitions and the physics of chemical diffusion and mixing. We will be rather formal and refer the applications and illustrations to other chapters of this Treatise (e.g., Chapter 11 and Chapter 12). Our goal is to explain why and when the advection diffusion equation can be used in mantle dynamics. The irreversible thermodynamics of multicomponent flows is discussed in various classical books (e.g., *Haase*, 1990; *de Groot and Mazur*, 1984). However as usual with geophysical flows, the mantle has many simplifications and a few complexities that are not necessarily well documented in these classical textbooks.

The second case will be for two phase flows in which the two phases are sepa-

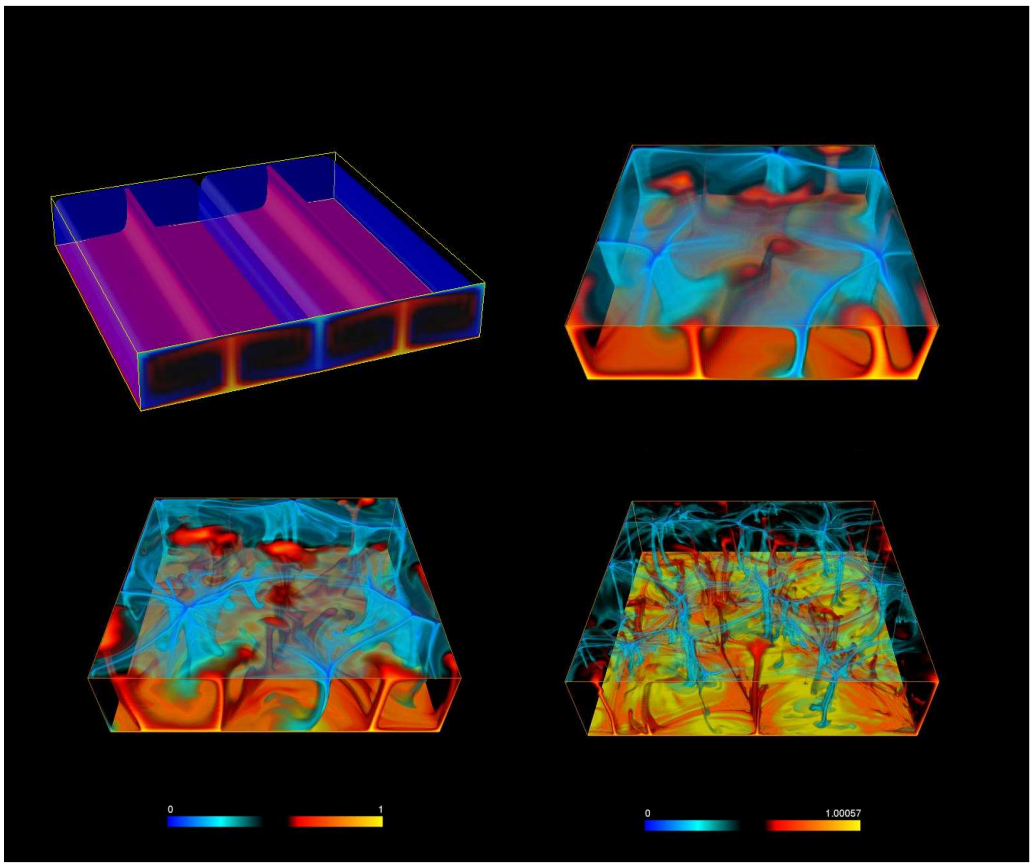


Figure 4: Convection patterns of a fluid heated from below at Rayleigh number $10^5$, $10^6$, $10^7$, $10^8$. The temperature color bars range from 0 (top boundary) to 1 (bottom boundary). The Boussinesq approximation was used (numerical simulations by F. Dubuffet). The increase in Rayleigh number corresponds to a decrease of the boundary layer thicknesses and the width of plumes. Only in the case of the lowest Rayleigh number (top left) is the convection stationary with cells of aspect ratio $\sim \sqrt{2}$ as predicted by marginal stability. For higher Rayleigh number, the patterns are highly time-dependent.